Supporting Information

Revealing the NIR Triggered Chemotherapy Therapeutic Window of Magnetic and Thermoresponsive Nanogels

Catalina Biglione,†[a,b,c] Julian Bergueiro,†[a,d] Stefanie Wedepohl,[a] Bastian Klemke,[e] Miriam C. Strumia*[b,c] and Marcelo Calderón*[a,f,g]

Outline

Figure S14. Confocal images after 12 hours incubation with Surebeads™, MNG, and Dox loaded MNGs in different volumes.

Figure S15. Confocal images after cell trypsinization, washing, and settle in magnetic tray of Surebeads™, MNG, and Dox loaded MNGs in different volumes.

Figure S16. Biodistribution of MNG measured by MRI.

Figure S17. Images of MNG distribution per organ measured by MRI (T2).

Figure S18. Z-Slices of MNG distribution in tumor 12h after injection measured by MRI (T2).

Figure S19. Individual relative tumor volumes per group in i.v. administration.

Figure S20. Individual relative tumor volumes per group in i.t. administration.

Figure S21. Mean body weight change for (a) intravenously and (b) intratumoral administered nanogels.

Table S1. Kinetics data of Dox release from MNG at different pHs and temperatures

pH	T (°C)	Zero order		First order		Higuchi		Korsmeyer−Peppas			Hixson-Crowell	
		K_1	R^2	K_1	R^2	K_H	R^2	K_{KP}	n	R^2	K_{HC}	R^2
4.2	37	7.3E-2	0.39	9.2E-4	0.43	1.54	0.65	1.2E4	11.66	0.90	1.3E-3	0.42
	50	0.16	0.52	2.5E-3	0.64	3.17	0.77	1.5E6	22.62	0.94	3.4E-3	0.60
5	37	0.11	0.68	1.4E-3	0.73	2.00	0.89	6.46	13.59	0.98	1.9E-3	0.72
	50	0.16	0.62	2.3E-5	0.70	3.08	0.86	2.62	21.00	0.99	3.2E-3	0.67
6	37	0.04	0.89	4.6E-4	0.90	0.74	0.98	0.06	4.59	0.90	7.0E-4	0.89
	50	0.05	0.71	4.6E-4	0.73	0.89	0.92	0.16	5.92	0.97	8.0E-4	0.73
7.4	37	0.04	0.69	4.6E-4	0.504	0.74	0.91	0.60	4.98	0.98	6.0E-4	0.70
	50	0.07	0.58	9.0E-3	0.61	1.40	0.83	1.53	9.88	0.98	1.2E-2	0.60

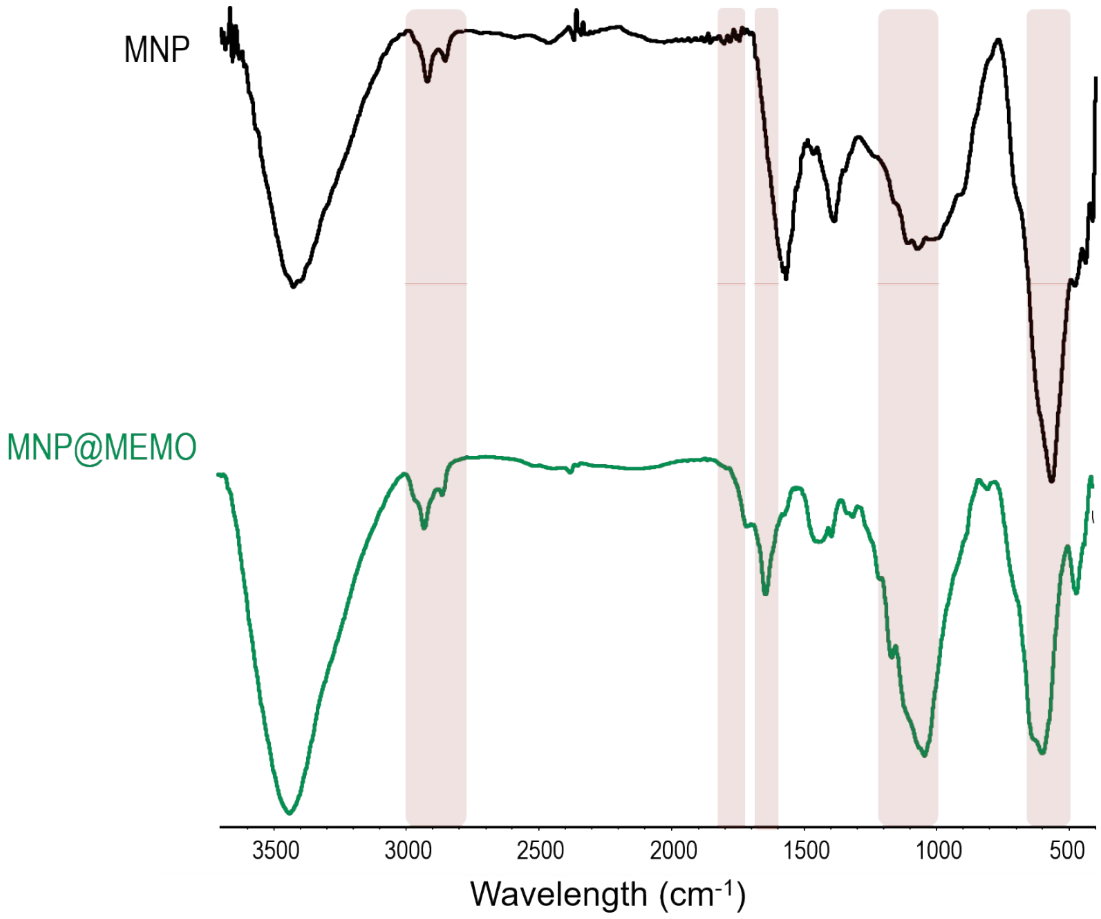

Figure S1. FT-IR spectra of MNPs and MNP@MEMO.

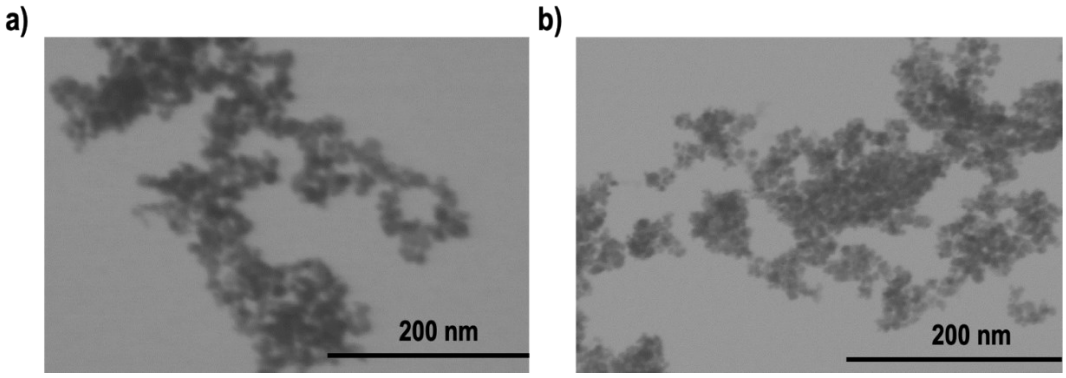

Figure S2. TEM images of a) MNPs and b) MNP@MEMO.

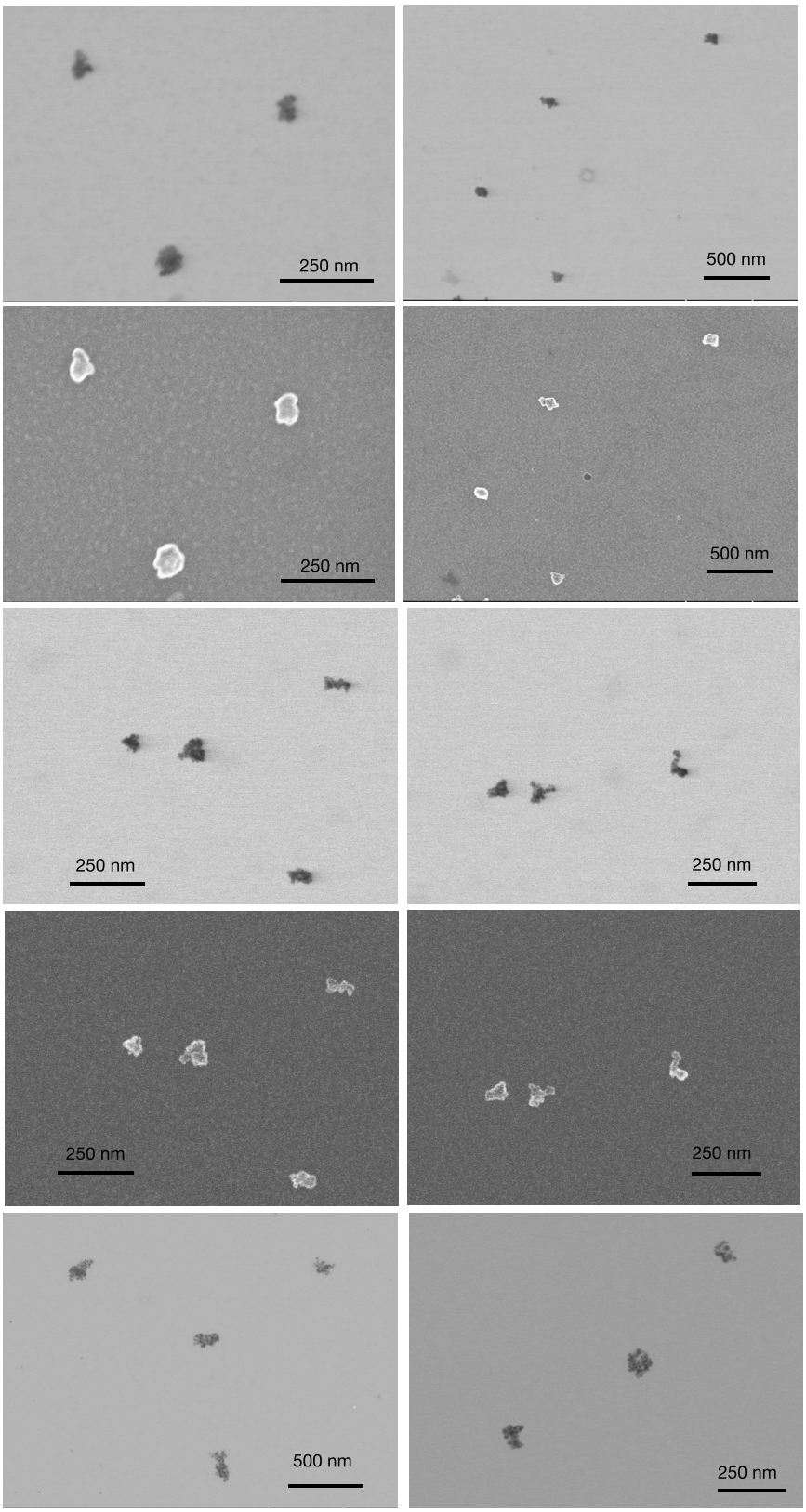

Figure S3. TEM and SEM images from MNGs used for size distribution calculation.

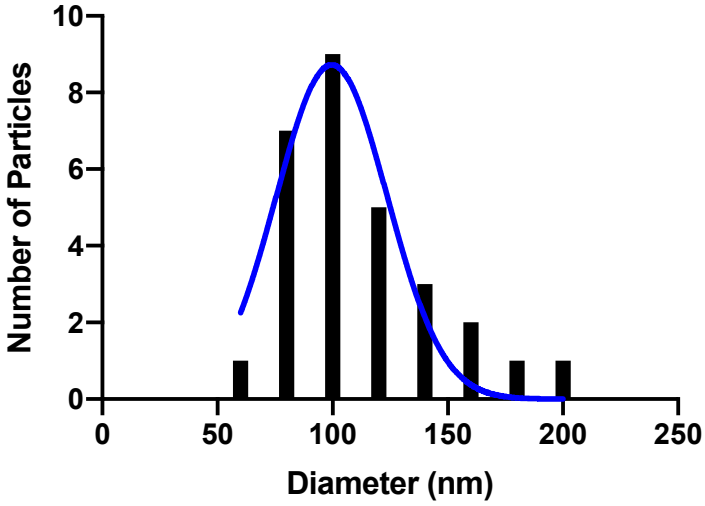

Figure S4. Size distribution analysis from TEM images. Mean: 99.2 nm, SD: 24.9 and PDI: 0.24.

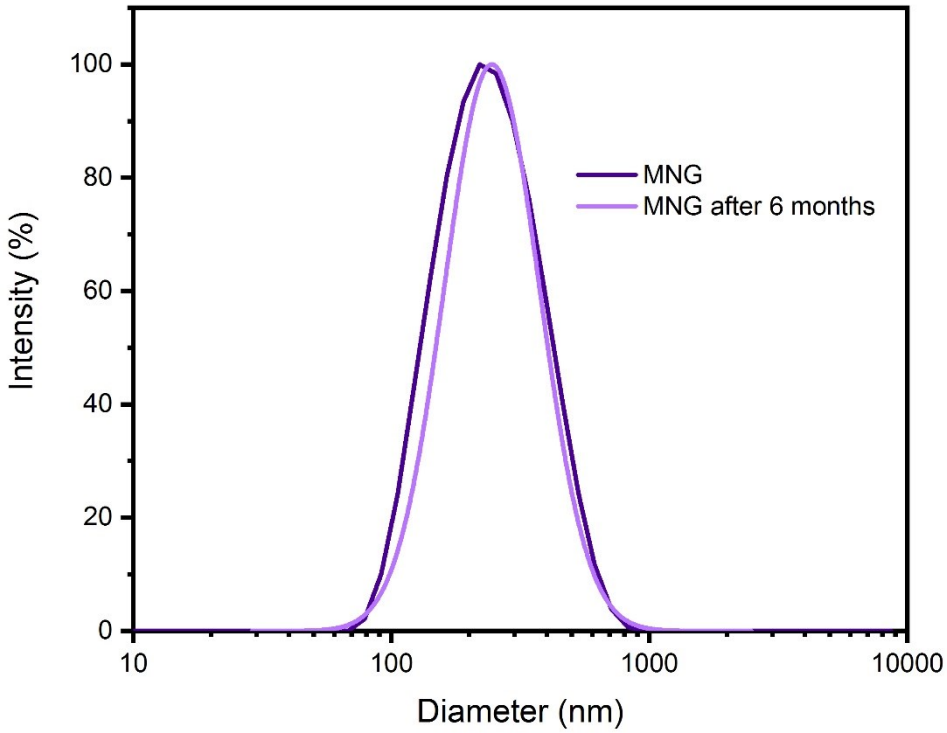

Figure S5. DLS measurement of MNG direct after purification and after six months

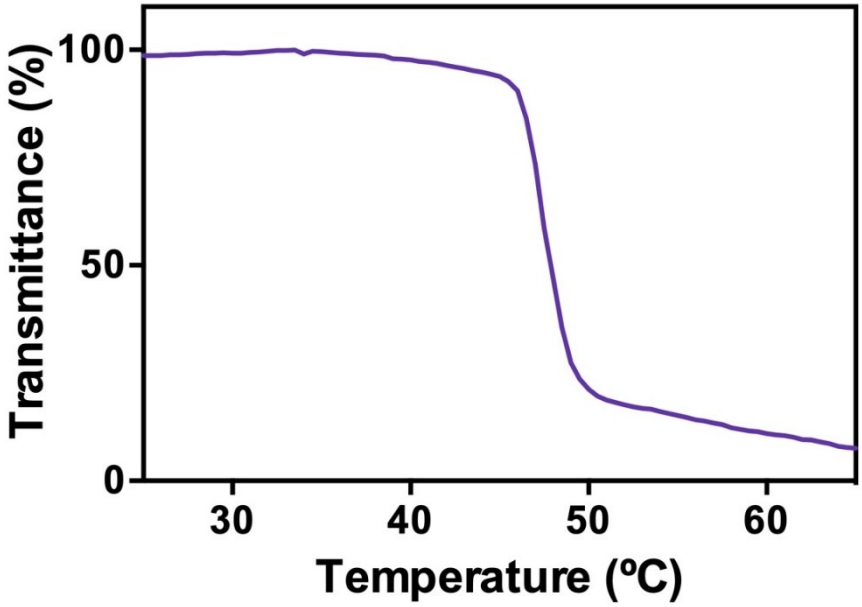

Figure S6. Transmittance of 600 nm light measured against the temperature for MNG.

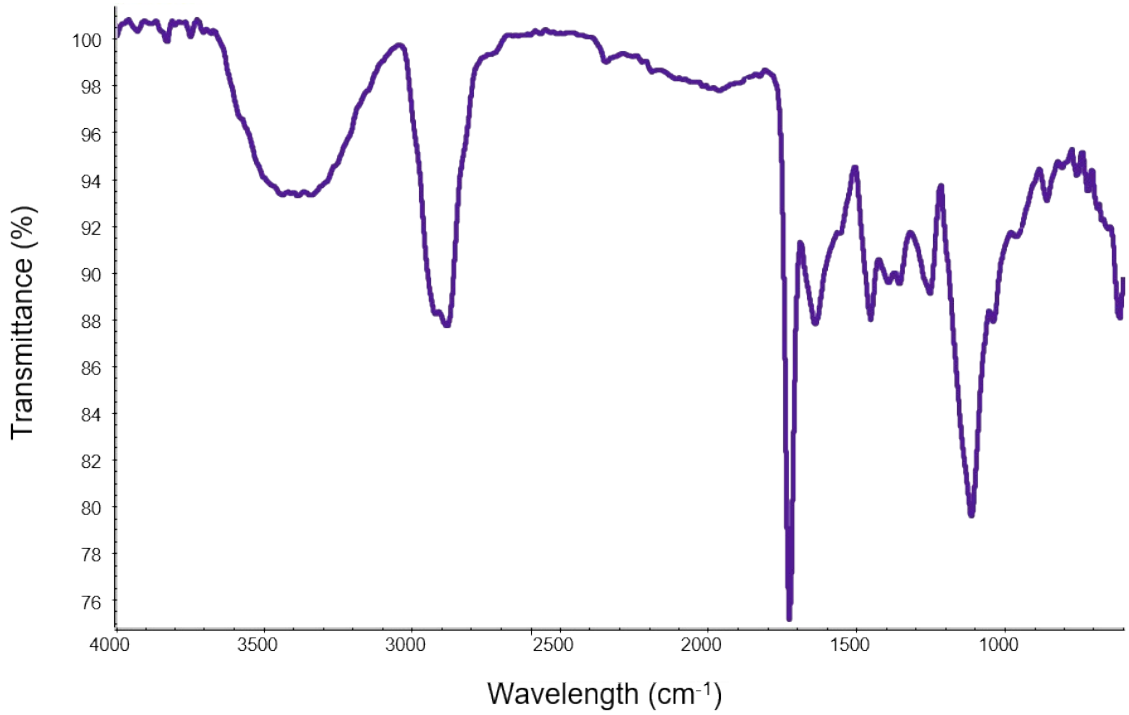

Figure S7. FT-IR spectrum of MNG.

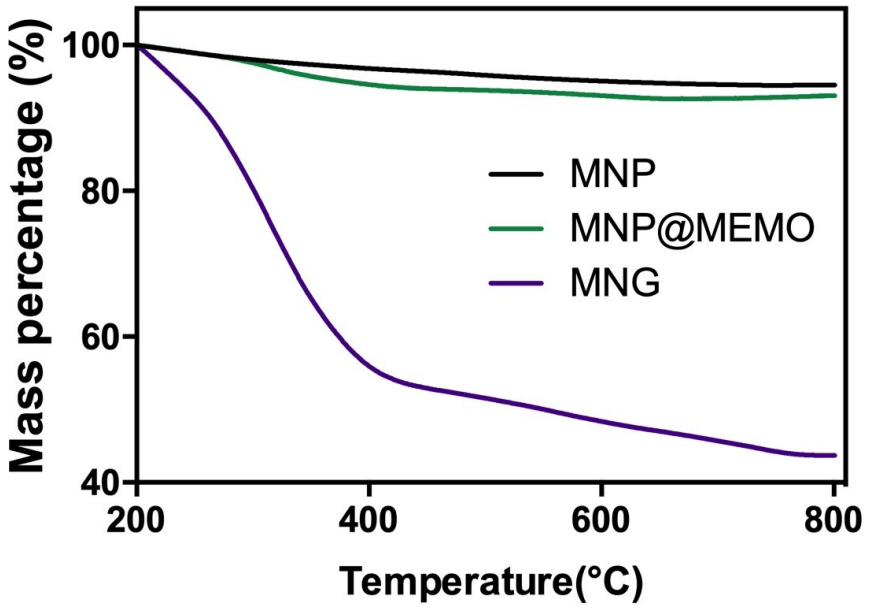

Figure S8. Thermogravimetric analysis of MNP, MNP@MEMO and MNG.

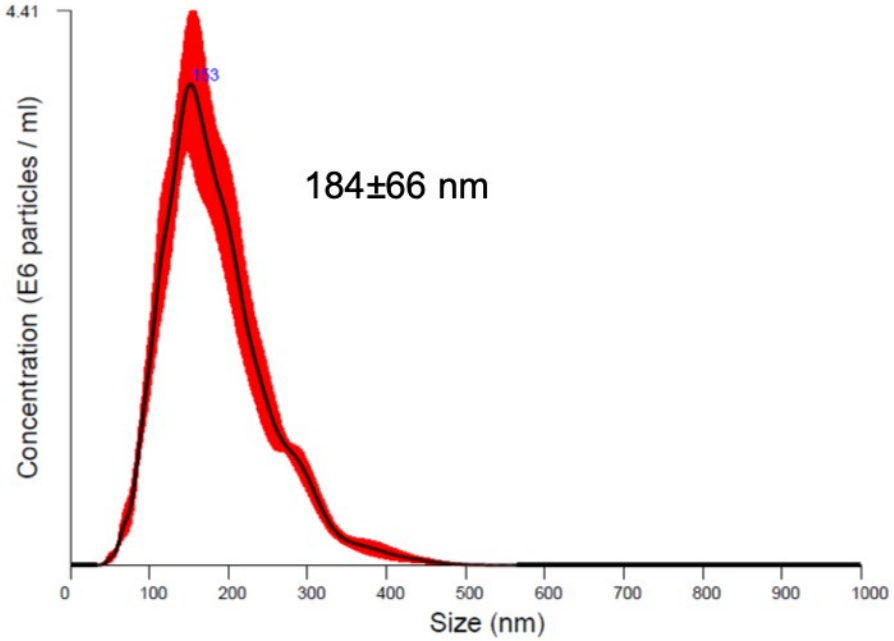

Figure S9. Nanoparticle Tracking Analysis experiments of MNG.

.

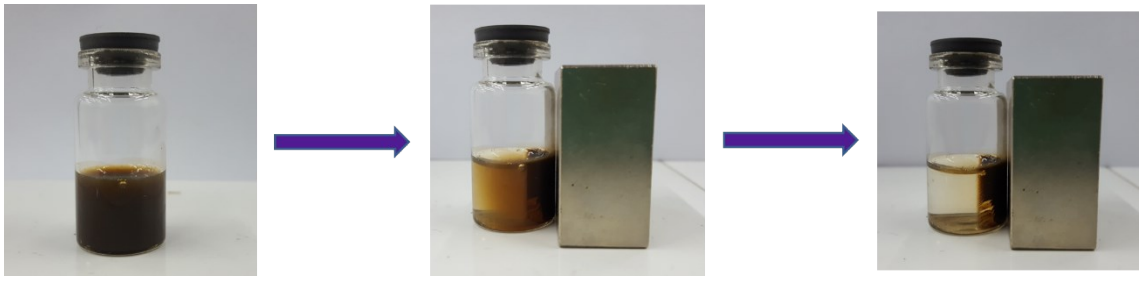

Figure S10. Images of a dispersion of MNG (1.6 mg / mL) exposed to a magnetic field at different times 0, 30 and 60 s.

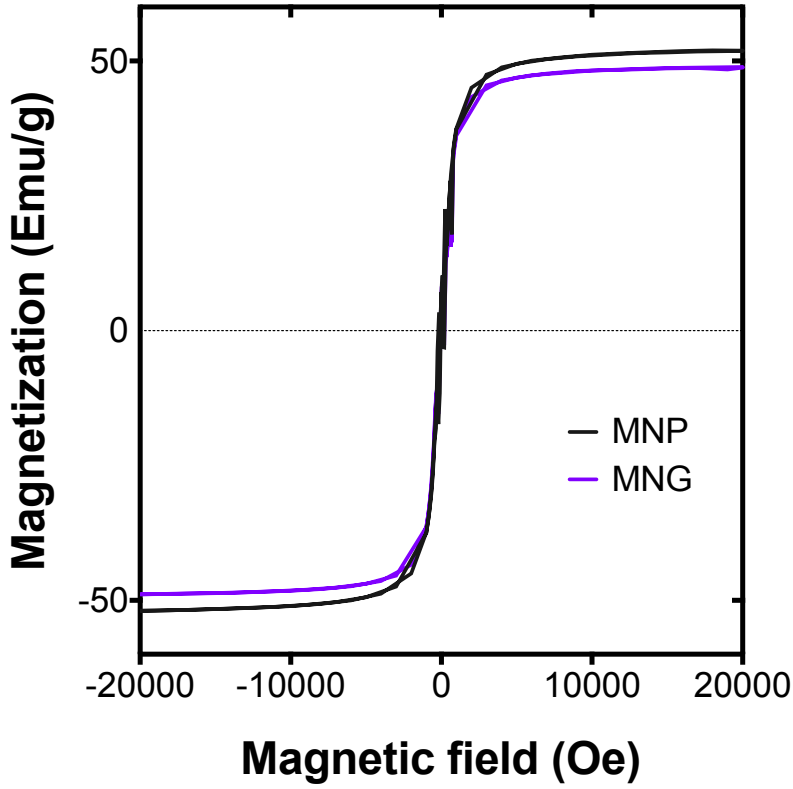

Figure S11. Comparison of the magnetization curves of MNP@MEMO and normalized MNG (considering the inorganic weight content of 43.8% by TGA) at 27 °C.

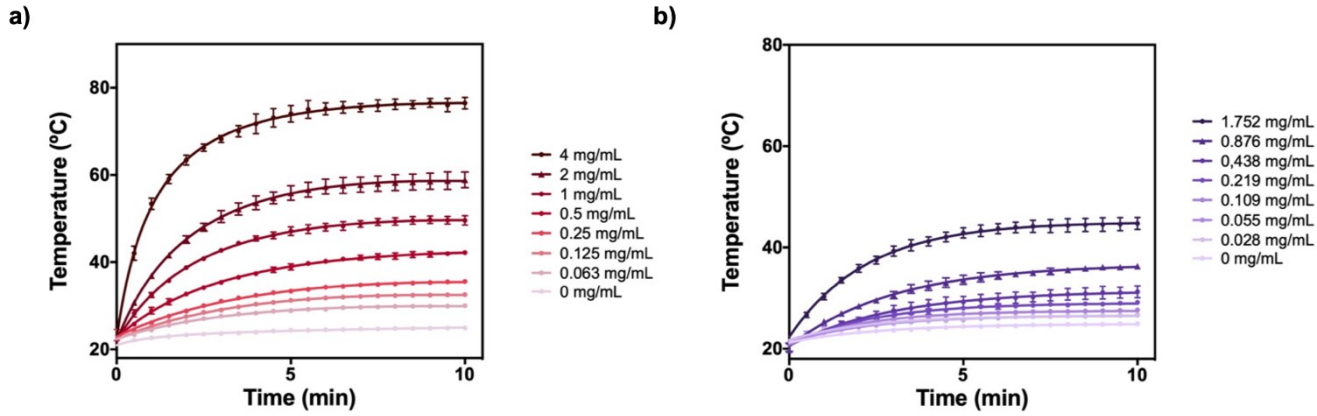

Figure S12**.** Heating curves under 10 minutes NIR laser irradiation of MNG and MNP@MEMO normalized to the MNPs content (data calculated from TGA measurements).

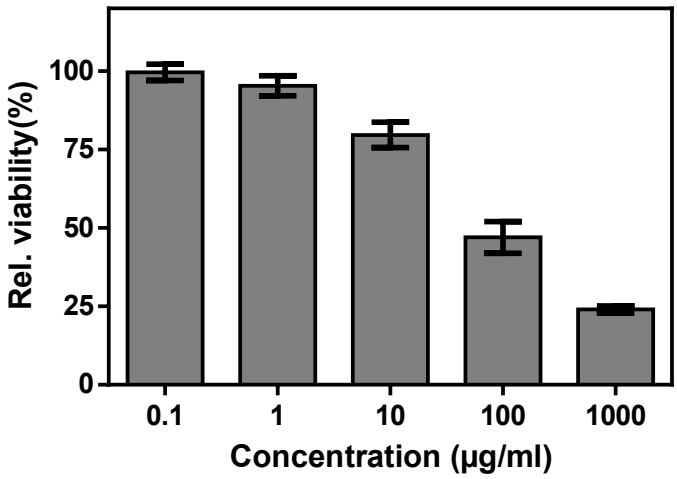

Figure S13. Relative viabilities of HeLa cells treated with increasing concentrations of MNG for 48h as determined by MTT test.

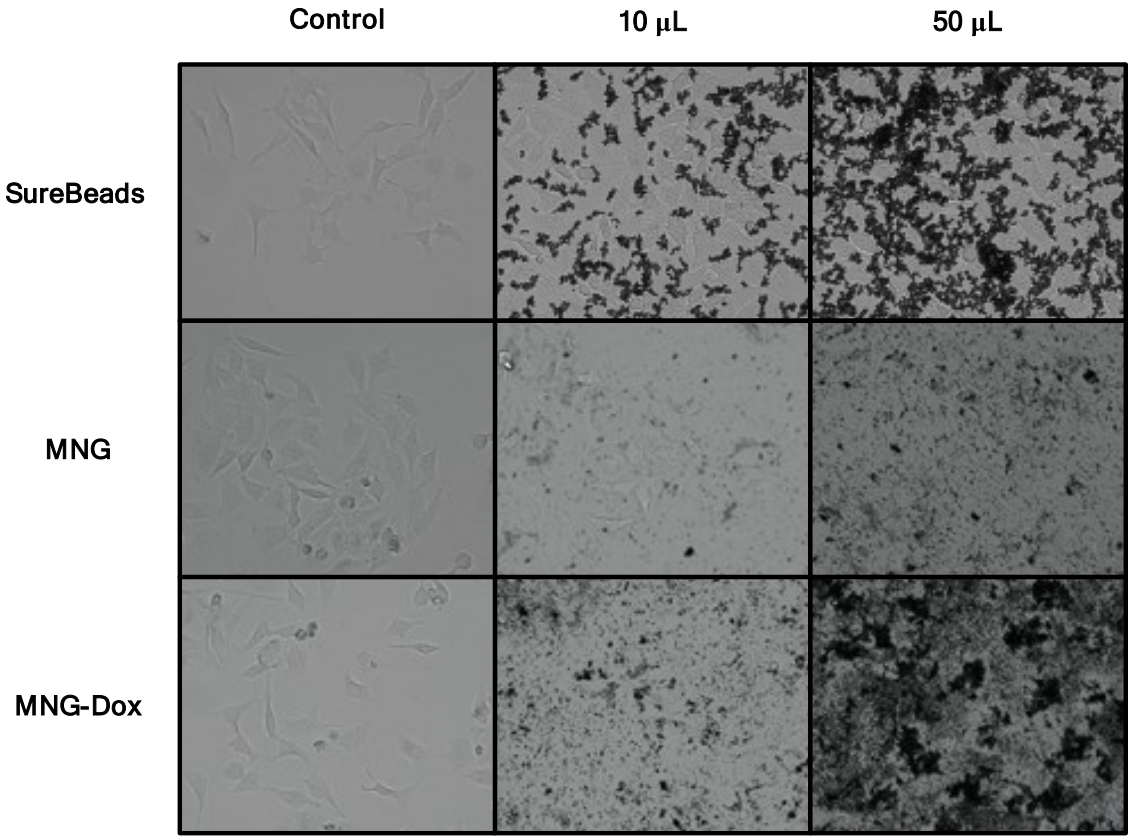

Figure S14. Confocal images after 12 hours incubation with Surebeads™, MNG, and Dox loaded MNGs in different volumes (10 μL and 50 μL) of a MNG solution of 10 mg/mL in $1x10^6$ HeLa cells.

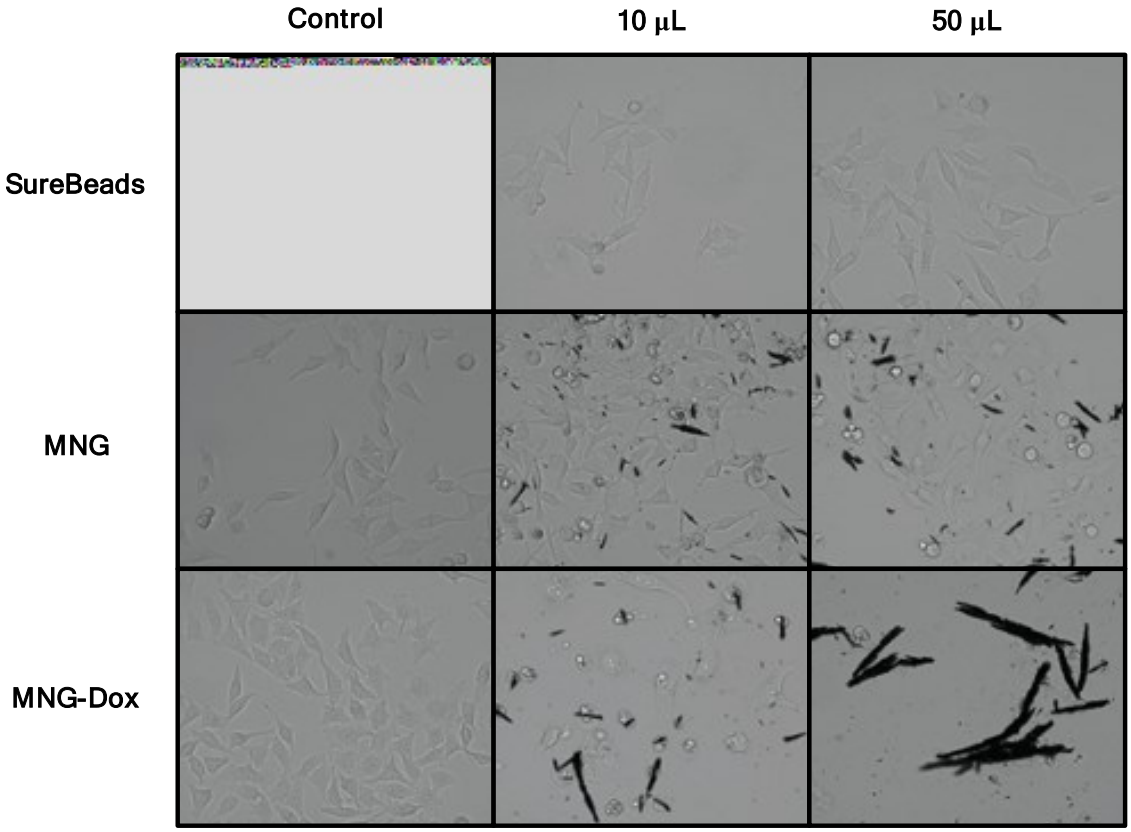

Figure S15. Confocal images after cell trypsinization, washing, and settle in magnetic tray of Surebeads™, MNG, and Dox loaded MNGs in different volumes (10 μL and 50 μL) of a MNG solution of 10 mg/mL in $1x10^6$ HeLa cells.

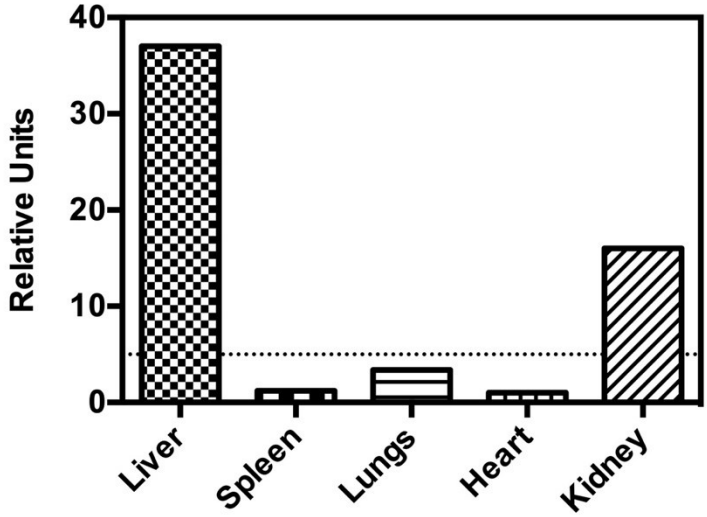

Figure S16. Biodistribution of MNG measured by MRI.

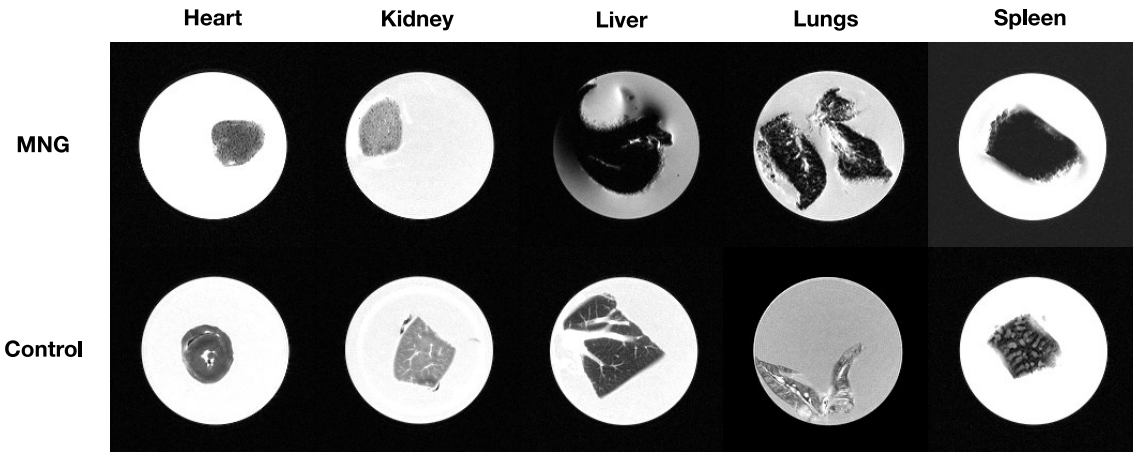

Figure S17. Images of MNG distribution per organ measured by MRI (T2).

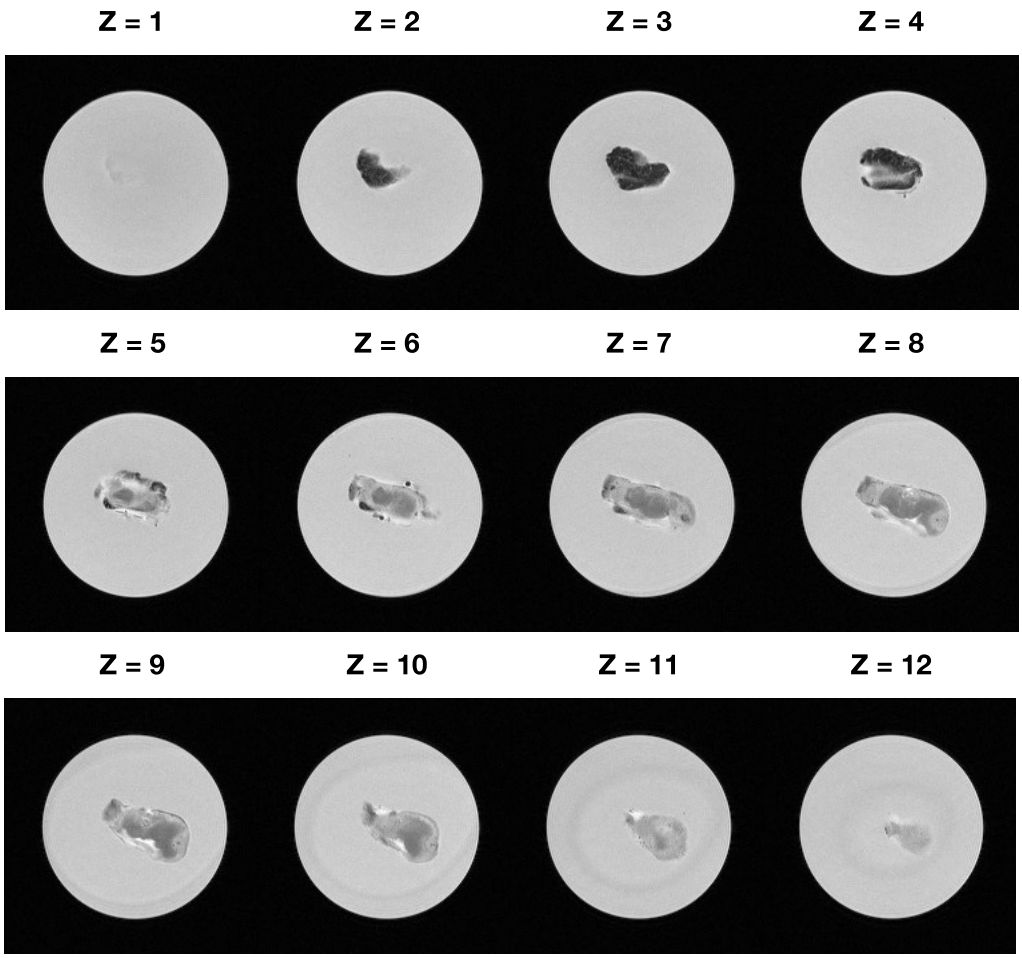

Figure S18. Z-Slices of MNG distribution in tumor 12 h after injection measured by MRI (T2).

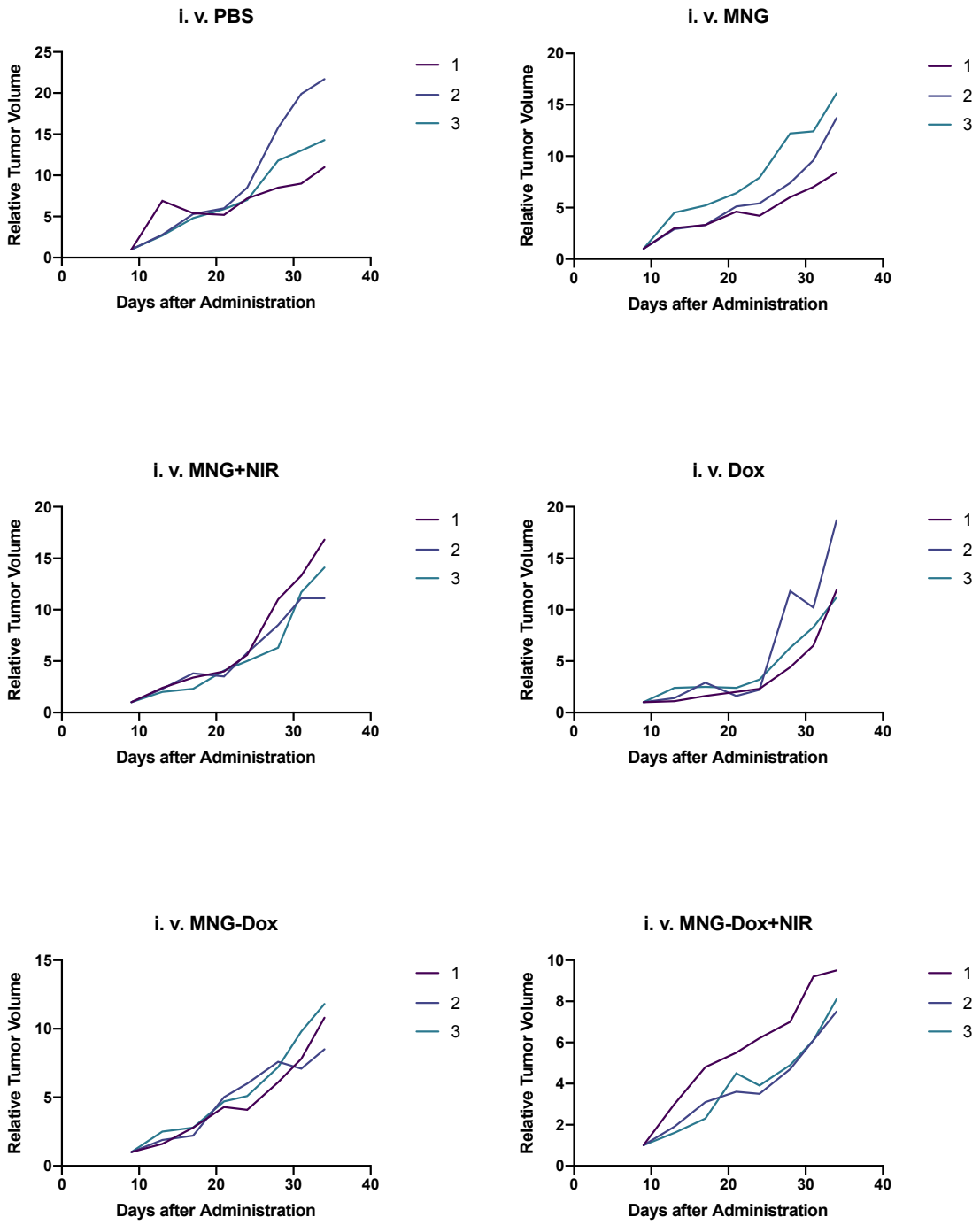

Figure S19. Individual relative tumor volumes per group in i.v. administration.

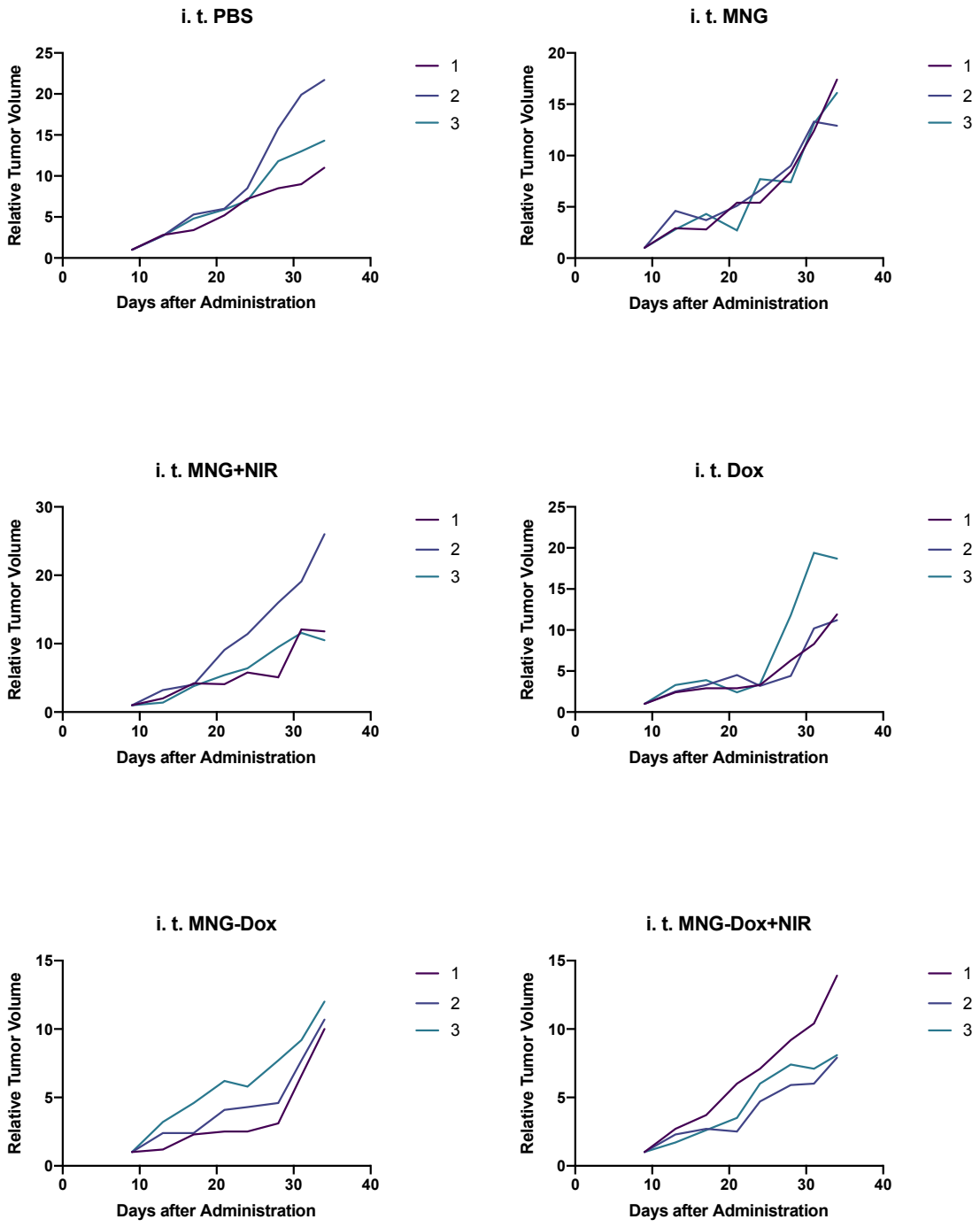

Figure S20. Individual relative tumor volumes per group in i.t. administration.

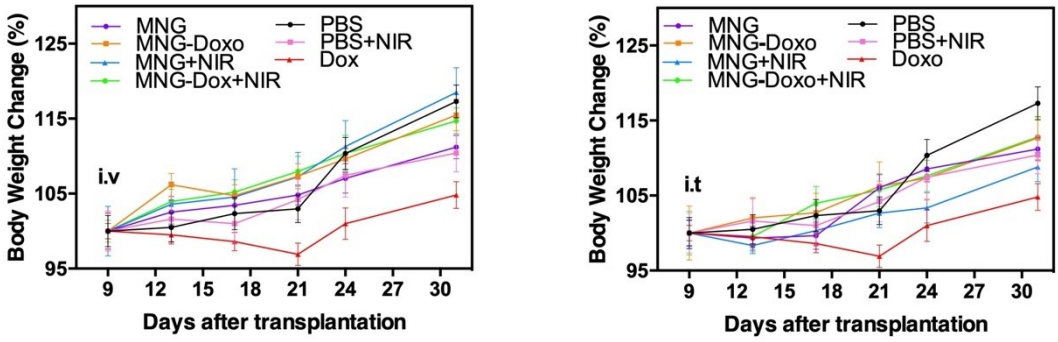

Figure S21. Mean body weight change for (a) intravenously and (b) intratumorally administered nanogels and controls.